communications physics

Article

A Nature Portfolio journal

https://doi.org/10.1038/s42005-026-02573-z

Chiral damping with persistent edge states from the interplay of topologies in open quantum systems

Ronika Sarkar[1,2], Suraj S. Hegde[3], Awadhesh Narayan[2] & Tobias Meng[4]

Open quantum systems are relevant for characterizing various phases of matter in a realistic setting. Yet, it remains unclear how dissipation-driven phenomena of boundary accumulation, known as the non-Hermitian skin effect and robust edge states of topological phases, synergise in a system. We study the dynamical consequences of combining the two effects in a paradigmatic Hofstadter model under dissipation. The time-dependent particle density exhibits both chiral damping, caused by the skin effect, and edge-selective extremal damping, rooted in the edge states. We further show that the time scales of the two processes decouple due to boundary-induced spectral topology, enabling both effects to appear clearly in the dynamics. We identify intermediate magnetic fields as the most favorable regime, since chiral damping is then partially recovered. Our results offer a direct dynamical probe of intertwined spectral and band topologies and are relevant for the design of robust quantum channels.

The topological characterization of matter has gained relevance beyond quantum materials, and is now also applied in photonic[1,2], mechanical[3,4], soft matter[5], and dissipative systems[6–8]. Often, the salient physics can at least approximately be described by non-Hermitian matrices. The interplay of such non-Hermitian "Hamiltonians" with topology is therefore under intense investigation. As a prominent example, the non-Hermitian skin effect (NHSE) is rooted in a topological winding of the complex spectrum of non-Hermitian matrices ("spectral topology"), rather than the topology of eigenstates ("band topology")[9–16]. In open quantum systems, the NHSE of damping generators manifests as a chiral damping wavefront in the dynamics[17,18].

In general, the spectral and band topologies of effective non-Hermitian systems can both be trivial or non-trivial. Non-Hermitian Hamiltonians can for example be associated with finite Chern numbers and have topological edge states[19]. In open quantum systems, this can lead to edge-selective extremal damping, a phenomenon in which particles resist dissipation predominantly at one or several edges of the system[20–22]. Some aspects of the interplay of NHSE and edge modes have been studied earlier. It was found that these effects compete, which can dramatically alter the localization of topological edge states[23–26].

The combined dynamical consequences of the NHSE and topological edge states in Lindbladian dynamics, however, remain unexplored. A central aspect in closing this knowledge gap is that dynamics is governed not only by the localization of eigenstates, but also by their complex spectrum. Extremal edge modes and chiral damping have been observed in different classes of systems, the former in examples with spectral line-gap topologies[20], and the latter with spectral point-gap topologies[22]. Our work advances the study of non-Bloch dynamics and topological edge modes[27,28] to a two-dimensional setting, where additional phenomena emerge. By introducing dissipation to an initially Hermitian Hamiltonian, we realize non-Hermitian spectral topology originating from the system's open dynamics rather than from inherent non-Hermiticity. The 2D Hofstadter model enables the controlled interplay between band topology and non-Hermitian spectral topology through magnetic flux, giving rise to edge-localized spectral structures, damping gaps, and potential higher-order boundary modes, unattainable in one dimension. In this work, we show that chiral damping and edge-selective extremal damping can coexist in open quantum systems due to a non-trivial interplay of (i) spectral topology in the bulk giving rise to an NHSE, (ii) band topology in the bulk giving rise to topological edge states, and (iii) spectral topology at the edge giving rise to a damping gap and minimal damping of the edge states. In addition, we explain how the time-evolution of particle densities provides a convenient probe of these different topologies.

Results and discussion

We analyze how bond dissipators, an important and broad class of dissipators, affects the dynamics of topologically non-trivial systems with edge

[1]Department of Physics, Indian Institute of Science, Bengaluru, India. [2]Solid State and Structural Chemistry Unit, Indian Institute of Science, Bengaluru, India. [3]Indian Institute of Science Education and Research Thiruvananthapuram, Vithura, India. [4]Institute of Theoretical Physics and Würzburg-Dresden Cluster of Excellence ct.qmat, Technische Universität Dresden, Dresden, Germany. e-mail: tobias.meng@tu-dresden.de

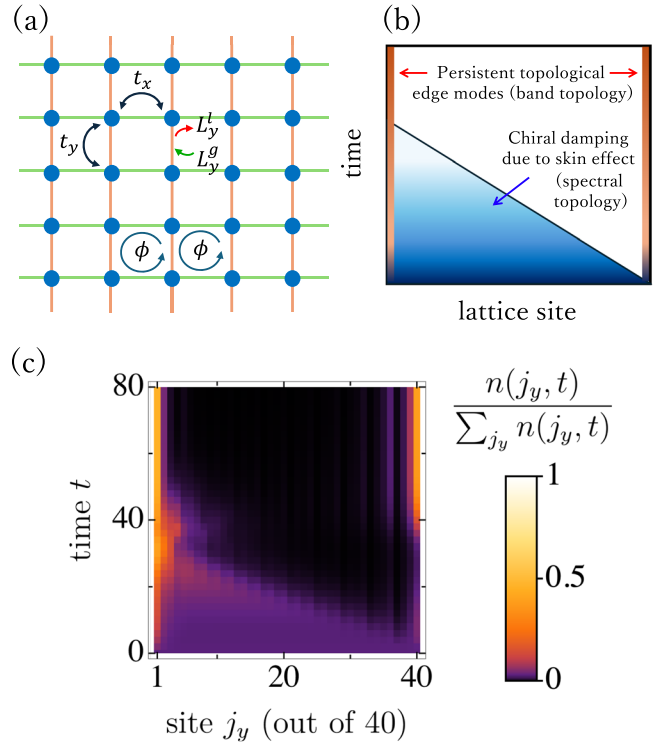

Fig. 1 | System and main results. a Dissipative Hofstadter model with hoppings t_x and t_y, dissipators L_y^l (loss) and L_y^g (gain) on y-bonds, and enclosed magnetic fluxes ϕ per plaquette. **b** Schematic illustration of the coexistence of skin effect and topological edge modes. **c** Time evolution of the particle number $n(j_y, t)$ in the tight-binding model. (The normalized particle number is indicated through the color bar.) We used periodic boundary conditions along x (summing 40 k_x-momenta per site), open boundary conditions along y (with $L_y = 40$ sites and site index j_y). The system is fully occupied at $t = 0$, and $\gamma^l = 0.2$, $\gamma^g = 0$, $\phi/\phi_0 = 1/4$, and $t_x = t_y = 1$.

states. As a main result, we find that topological edge states form the dominantly occupied states in the dynamics of topological systems with bond dissipation. To illustrate our findings, we focus on the paradigmatic Hofstadter model[29] coupled to an environment inducing gain and loss along the y-bonds, see Fig. 1a, but we also comment on the broader applicability of our results. Our central findings are as follows: (A) Since bulk sites have more attached bonds than edge sites, bond dissipation generically gives rise to weaker dissipation at the edges than in the bulk. Physically, this implies that the states localized at the edges tend to have the lowest decay. (B) At the same time, bond dissipation is well-known to induce an NHSE[10–12], and we observe the corresponding chiral damping wavefront in the bulk[17,18]. The edge states, however, experience a competition of topological and skin localizations, both exponential. For sufficiently small dissipation, the edge states resist skin localization[23–26]. We then find that particle localization at the edges persists even at long times, rendering the topological edge states the dominantly occupied states in the system dynamics. (C) This physics can be detected via the spatially resolved particle density in the system, as schematically illustrated in Fig. 1b, explaining the main features of a numerical simulation shown in Fig. 1c. (D) We connect our concrete results to a general discussion of the interplay of spectral and band topologies, explaining how our findings pertain to dynamics in open quantum systems more broadly.

General formalism

A general Hermitian system Hamiltonian can be expressed in the second quantised form as: $H = \sum_{\alpha\beta} c_\alpha^\dagger h_{\alpha\beta} c_\beta$. We assume that this Hamiltonian is topologically non-trivial (later we consider a concrete example of the Hermitian Hofstadter model). The environment is introduced in the language of a Lindblad Master equation for the system's density matrix ρ[30,31]:

$$\frac{d\rho}{dt} = -i[H,\rho] + \sum_\alpha \left(L_\alpha \rho L_\alpha^\dagger - \frac{1}{2}\{L_\alpha^\dagger L_\alpha, \rho\} \right) \tag{1}$$

The effect of dissipations is modeled by linear jump operators which can be expressed in the most general form as $L_\nu^g = \sum_i D_{\nu,i}^g c_i^\dagger$ and $L_\nu^l = \sum_i D_{\nu,i}^g c_i$, corresponding to gain and loss type dissipation, respectively. For the remainder, it is helpful to define the matrices $M_{\alpha\beta}^g = \sum_\nu D_{\nu\alpha}^{g*} D_{\nu\beta}^g$ and $M_{\alpha\beta}^l = \sum_\nu D_{\nu\alpha}^{l*} D_{\nu\beta}^l$, which in turn allow the definition of the damping matrix X as

$$X = ih^T - (M^{l^T} + M^g) \tag{2}$$

These matrices are key for the dynamics of our main observable of interest, the covariance matrix C with matrix elements $C_{\alpha\beta}(t) = Tr(c_\alpha^\dagger c_\beta \rho(t))$. Its exact time evolution follows from Eq. (1), and is governed by ref. 17.

$$\frac{dC(t)}{dt} = XC(t) + C(t)X^\dagger + 2M^g, \tag{3}$$

The solution of Eq. (3) can be split into a constant steady-state value C_{ss} and the convergence towards the steady state as $C(t) = C_{ss} + \widetilde{C}(t)$. The time evolution of $\widetilde{C}(t)$ can be cast into an analytic expression in terms of the eigensystem of X,

$$\widetilde{C}(t) = \sum_{m,m'} e^{(\lambda_m + \lambda_{m'}^*)t} |\psi_{R,m}\rangle\langle\psi_{L,m}|\widetilde{C}(0)|\psi_{L,m'}\rangle\langle\psi_{R,m'}|, \tag{4}$$

where λ_m ($\psi_{R/L,m}$) denotes the m-th eigenvalue (right/left eigenvector) of the damping matrix X[17].

Interplay of spectral and band topologies

Our general model exhibits both spectral and band topologies. In our case, both topologies are hosted by the damping matrix X, but similar conclusions can also be drawn for non-Hermitian Hamiltonians and other non-Hermitian matrices.

Consider therefore in the first step some Hermitian matrix $\mathcal{M}$ representing a topological system with open boundary conditions along y (such as the damping matrix X at zero damping in our case, or the Hamiltonian for a topological system). In the second step, we assume the system to be coupled to some environment giving rise to non-reciprocal nearest-neighbor hoppings $t_y \pm \gamma$, which entails an NHSE along y. Due to the non-reciprocal hopping encoded by $\gamma \neq 0$, the system is now represented by a non-Hermitian matrix $\mathcal{M}_{nH}$. In the simplest cases, the non-Hermiticity corresponding to this non-reciprocity can be removed from $\mathcal{M}_{nH}$ by acting on it with a so-called imaginary gauge transformation (IGT), $\mathcal{M}_{nH}(t_y, \gamma) = S^{-1}\mathcal{M}_{nH}(\tilde{t}_y, 0)S$, where S implements the IGT and $\tilde{t}_y = \sqrt{t_y^2 - \gamma^2}$[10,32,33]. This transformation preserves the spectrum of $\mathcal{M}_{nH}$. Simultaneously, the transformation also affects the eigenstates by rescaling them with an exponential factor e^{y/ξ_S}, where $\xi_S = \left(\frac{1}{2}\log\frac{t_y-\gamma}{t_y+\gamma}\right)^{-1}$. Overall, the IGT thus trades a matrix with non-reciprocal hopping for a matric with reciprocal hopping, while at the same time giving an exponential factor to all the eigenstates to preserve the skin-localization.

Since the system is topological by assumption, bulk-boundary correspondence implies that the Hermitian matrix $\mathcal{M}(\tilde{t}_y, 0)$ generically has exponentially localized, topologically protected edge states. A reverse IGT then shows that while all extended bulk states of $\mathcal{M}(\tilde{t}_y, 0)$ correspond to skin-localized states of $\mathcal{M}(t_y, \gamma)$, the same need not be true for the edge states. Those instead, experience a competition between topological and skin localization: one edge mode is tightly localized, $e^{-y/\xi_S} e^{-y/\xi_R}$, while the other is stretched out, $e^{-y/\xi_S} e^{-(L-y)/\xi_L}$, where $\xi_{R/L}$ are the topological localization lengths. If $\xi_S \gg \xi_{R,L}$, i.e., for sufficiently weak non-reciprocity, both

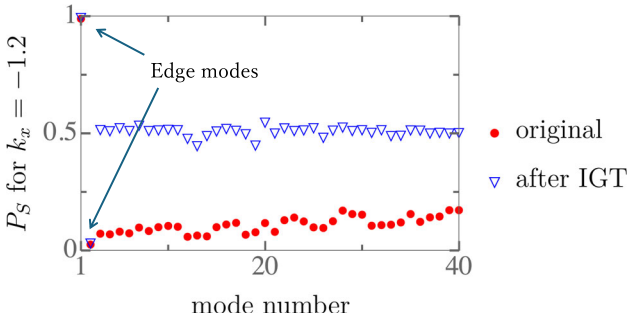

Fig. 2 | Deconstructing band topology and spectral topology. Static polarization P_S for the original eigenstates of the damping matrix X, and after effectively removing the non-Hermitian skin effect by the application of an imaginary gauge transformation only to X, but not to the eigenstates. Here, $\gamma^l = 0.2$, $\gamma^g = 0$, $\phi/\phi_0 = 1/4$, $t_x = t_y = 1$, and $L_y = 40$.

edge modes remain localized at their respective edges. Bulk band topology (giving rise to topological edge states) and bulk spectral topology (yielding a bulk NHSE) thus co-govern the spatial profile of eigenstates[23–26]. All eigenstates in our computations are obtained conventionally from the right eigenvectors of the non-Hermitian damping matrix X. Let us concretize the above discussion using a viable system and environment.

Model

We consider spinless electrons on a two-dimensional square lattice subject to a uniform magnetic field, see Fig. 1a. With the gauge choice $\mathbf{A} = B(-y, 0)$, applying Peierls substitution[29], and assuming cylindrical boundary conditions (periodic in x, open in y), the Hamiltonian takes the form

$$H = \sum_{k_x j_y} (2t_x \cos(k_x - 2\pi j_y \phi/\phi_0)\, c^\dagger_{k_x j_y} c_{k_x j_y} + t_y\, c^\dagger_{k_x j_y+1} c_{k_x j_y} + t_y\, c^\dagger_{k_x j_y} c_{k_x j_y+1}), \tag{5}$$

and is known as the Hermitian Hofstadter model[29]. $c^\dagger_{k_x j_y}$ are fermionic creation operators for an electron with x-momentum k_x and site number j_y along y. The hopping amplitudes are t_x, t_y, the magnetic flux per unit cell is ϕ, and $\phi_0 = h/e$ is the flux quantum.

The dissipation arising from the environment are modeled using bond dissipators

$$L^l_{k_x j_y} = \sqrt{\gamma^l}\,(c_{k_x j_y} - i c_{k_x j_y+1}), \tag{6a}$$

$$L^g_{k_x j_y} = \sqrt{\gamma^g}\,(c^\dagger_{k_x j_y} + i c^\dagger_{k_x j_y+1}). \tag{6b}$$

Here, γ^l (γ^g) represents the dissipation strength for loss (gain). For the Hofstadter model with bond dissipators the damping matrix reads

$$X = i H_{\mathrm{nH-Hof}} - 2\gamma\, \mathbb{1} + \gamma\, I_{\mathrm{edges}}, \tag{7}$$

where $\gamma = \gamma^g + \gamma^l$ and

$$H_{\mathrm{nH-Hof}} = \sum_{k_x j_y} \Big(2t_x \cos(k_x - 2\pi j_y \phi/\phi_0) c^\dagger_{k_x j_y} c_{k_x j_y} + (t_y + \gamma) c^\dagger_{k_x j_y+1} c_{k_x j_y} + (t_y - \gamma) c^\dagger_{k_x j_y} c_{k_x j_y+1} \Big). \tag{8}$$

is a non-Hermitian Hofstadter model with non-reciprocal hoppings. The term $\sim \mathbb{1}$ in Eq. (7) merely shifts the entire spectrum of X by 2γ, but leaves all eigenstates unaffected. In contrast, I_{edges} is a diagonal matrix with zeros everywhere except for unit entries at the top left and bottom right (corresponding to the edge sites). This term physically encodes the fact that edge sites have fewer attached bonds than bulk sites, and are consequently less affected by bond dissipators. We also note that the non-Hermiticity in the damping matrix arises due to the coupling with the environment—it directly follows from the master equation Eq. (1), and is not included ad-hoc. Physically, the non-Hermiticity of X represents the tendency of the system to decay towards its steady state. In particular, the imaginary nonzero parts of the eigenvalues of X encode the decay rates at which different modes relax or are damped through interaction with the environment. The dissipative nature and resulting steady-state behavior of the system are thus fully captured by the non-Hermitian structure of X.

The central interest of the present work is how the interplay of spectral and band topologies affects dynamics. To boost the impact of the rebellious topological edge states onto dynamics, the damping rates for bulk and edge states should differ significantly. In an initially Hermitian topological system, a corresponding gap in damping rates(i.e real part of X-spectrum) can be induced by adding dissipation only to the edges. Technically, this leads to a spectral point gap for the topological edge states[34]. Particularly, the boundaries of Hermitian topological phases under dissipation are known to host intrinsically non-Hermitian point-gap topological phases[34]. The key feature in such scenarios is the opening of a damping gap exclusively for the edge-states, thus stabilizing them dynamically. In open quantum systems, effective edge-only dissipation can readily be created by bond dissipators, since edge sites have less bonds attached than bulk sites.

It is now important to recall that (reverse) IGTs not only preserve the spectrum of $\mathcal{M}_{nH}$, but also its diagonal elements. Adding edge-only dissipation to either $\mathcal{M}_{nH}(\tilde{t}_y, 0)$ or $\mathcal{M}_{nH}(t_y, \gamma)$ consequently results in a damping gap (a finite separation between the least-damped and more strongly damped modes in the spectrum of a dissipative quantum system), for the topological edge states, but not for any other states. In particular, skin-localized bulk states of $\mathcal{M}_{nH}(t_y, \gamma)$ are essentially unaffected. Since the eigenvalues of X encode the decay rates of different modes toward the steady state, the damping gap (or Liouvillian gap)[35–37] quantifies the slowest (i.e., least negative real part) nonzero decay rate in the system. This gap sets the asymptotic rate at which perturbations relax: a finite damping gap implies exponential and rapid convergence to steady state, whereas a closing (vanishing) damping gap signals slow relaxation or possible long-lived modes. In the context of the interplay between chiral damping and topological edge modes, the Liouvillian gap controls how quickly dynamical signatures of both phenomena appear and how robustly they persist before the final steady state is reached.

Deconstructing damping effects in the spectrum of a dissipative Hofstadter model

The non-Hermitian Hofstadter model and related Aubry-André-Harper model have been studied before in the context of suppression of skin-effect and chiral damping as well as localization-delocalization transitions[38–48]. Chiral damping in open quantum systems refers to the emergence of a dissipative chiral wave-front with a velocity determined by the damping gap in the system and the underlying non-Hermitian skin-effect. Here, we are interested in how the interplay of spectral and band topologies affects dynamics, especially at intermediate magnetic fields (we comment on weak fields later). We first analyze the spatial localization of the eigenstates of X, captured by the spectral polarization

$$P_S(m, k_x) = \frac{1}{L_y} \sum_{j_y=1}^{L_y} j_y\, |\psi_{R,m}(k_x, j_y)|^2. \tag{9}$$

Here, we used translation invariance along x to decompose the problem into decoupled k_x-sectors. In our numerical implementations, we normalize the right eigenstates as $\sum_{j_y} |\psi_{R,m}(j_y, k_x)|^2 = 1$. Figure 2 shows the spectral polarization in a parameter regime supporting topological edge states. To allow a convenient identification of bulk and edge states, we depict P_S in the original model (red dots), and also after removing the NHSE using

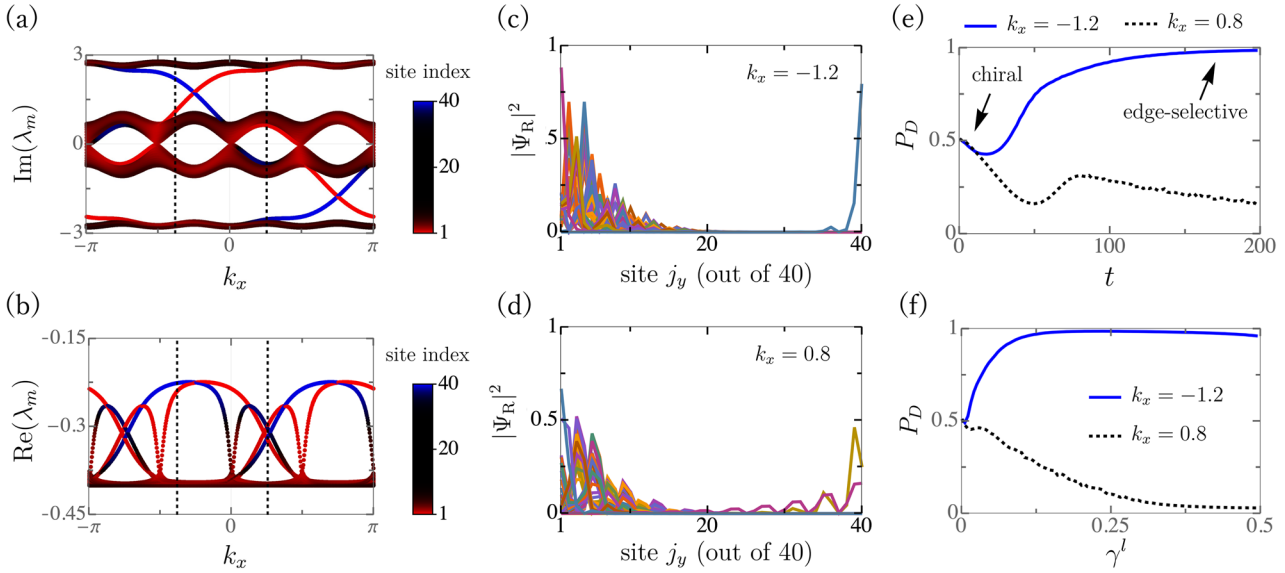

Fig. 3 | Dynamics: coexistence of topological edge modes and skin-localized bulk modes. a, **b** Imaginary and real parts of λ_m (eigenvalues of X). Colors indicate the site index expectation value of the corresponding right eigenstates, vertical lines mark momenta $k_x = -1.2$ and $k_x = 0.8$. **c**, **d** Spatial profile of the eigenstates for $k_x = -1.2$ and $k_x = 0.8$. **e** Dynamical polarization as a function of time. **f** Dynamical polarization as a function of damping at fixed time $t = 200$. Here, damping rate $\gamma^l = 0.2$ except for (**f**), dissipation strength $\gamma^g = 0$, magnetic flux $\phi/\phi_0 = 1/4$, couplings $t_x = t_y = 1$, and lattice length $L_y = 40$.

an ad-hoc modified IGT (blue open triangles). More concretely, we apply the IGT only to the damping matrix and then calculate the eigenstates of this transformed matrix without including the exponential localization factor of the eigenstates responsible for the NHSE. As heralded by a value of $P_S \approx 0$, the NHSE localizes most eigenstates of the damping matrix X at one edge. In striking contrast, the topological edge states (modes number 1 and 2 in Fig. 2) remain well-localized at their respective edges despite the NHSE. After performing the modified IGT (blue triangles in Fig. 2), almost all states are localized in the bulk with intermediary P_S values due to the removal of NHSE, and the two topological edge states are localized at the two opposite edges with $P_S = 1$ and 0, as expected. This shows that the edge localization due to topological edge physics, and the edge localization due to the NHSE are essentially independent and superimposed.

Next, we turn to the dynamics of electronic densities. The momentum-resolved time-dependence is described by the dynamical polarization, defined as

$$P_D(k_x, t) = \frac{1}{L_y} \frac{\sum_{j_y=1}^{L_y} j_y \, n(k_x, j_y, t)}{\sum_{j_y=1}^{L_y} n(k_x, j_y, t)}. \tag{10}$$

Here, the time-dependent local density $n(k_x, j_y, t)$ is simply the diagonal element of $C(t)$ with $\alpha = \beta = (k_x, j_y)$. Since Eq. (7) contains a term corresponding to edge-only dissipation, our general discussion implies that the edge states exhibit a damping gap. This is shown in the k_x-resolved spectrum of the damping matrix in Fig. 3a–b. The imaginary part of the spectrum reflects the band-structure of the Hofstadter model. Topological edge states crossing the band gaps are clearly visible in Fig. 3a around $k_x \approx -0.8$ and $k_x \approx 2.4$. The real part of the spectrum depicted in Fig. 3b shows that edge-only dissipation induces a damping gap for these edge states. A simple perturbative argument indicates that the edge-state damping gap is of order γ, in agreement with our numerical findings. For all time-evolution calculations, we initialize the system with a lattice configuration in which each site is singly occupied.

Due to this damping gap, the edge states govern the long-time dynamics. We show this using two representative momenta: well-defined topological edge states exist for $k_x = -1.2$, while they are not well-separated from bulk states for $k_x = 0.8$, as visible from Fig. 3(a)–(b), and further illustrated in Fig. 3c–d showing the spatial profile of the right eigenstates of X. Note that for a fixed k_x, different edge states in general have different distances to the bulk states. This results in different localization lengths and different damping gaps. The long-time dynamics for fixed k_x is governed by the single edge state with the lowest damping. Figure 3(e) presents the time-dependence of P_D. We find that the chiral damping rooted in the NHSE of X leads to an initial linear evolution (here: decrease) of the dynamical polarization. In contrast, the long-time dynamics depends on whether well-defined edge states with a damping gap are present or not: if present, such edge states lead to edge-selective extremal damping – an open system quantum phenomenon where dissipation is either maximized or minimized specifically at the system's boundaries, which renders topological edge states as the ones with maximal or minimal damping[20]. To assess the robustness of this effect with varying dissipation, we plot the polarization at the late time $t = 200$ as a function of the damping γ in Fig. 3f. For $k_x = -1.2$, we find that P_D first settles to 1, heralding edge-selective extremal damping, but decreases as the NHSE becomes stronger at larger γ, which reduces the localization of the edge state. For $k_x = 0.8$, on the contrary, edge-selective extremal damping is absent due to the absence of well-defined damping gap for the edge states. This demonstrates that well-defined topological edge states are indeed resilient against skin localization, and that they facilitate edge-selective extremal damping due to their damping gap. Particles will consequently predominantly remain at the edges at late times.

The momentum-resolved analysis of Fig. 3 can be generalized to more accessible observables. For the setting of Fig. 1, the momentum-summed local densities $n(j_y, t) = \sum_{k_x} n(k_x, j_y, t)$, summed over 40 equidistant k_x-values, exhibit two different regimes. After preparing the system in a fully occupied state, the short-time dynamics is governed by an emptying of the bulk states via a chiral damping wavefront, see Fig. 1c. The topological edge states, however, govern the long-time dynamics due to their damping gap: only particles at the edges remain in the system at long times. This illustrates that local particle densities are a convenient probe for the coexistence of spectral topology and band topology. While the robust edge modes originate from the band topology of the underlying Hermitian Hamiltonian, the spectral topology governs how dissipation and non-Hermiticity shape dynamical features like directional (chiral) damping.

Magnetic field-dependence of skin localization

The NHSE is known to be suppressed by weak magnetic fields because spatially localized Landau level states differ dramatically from extended

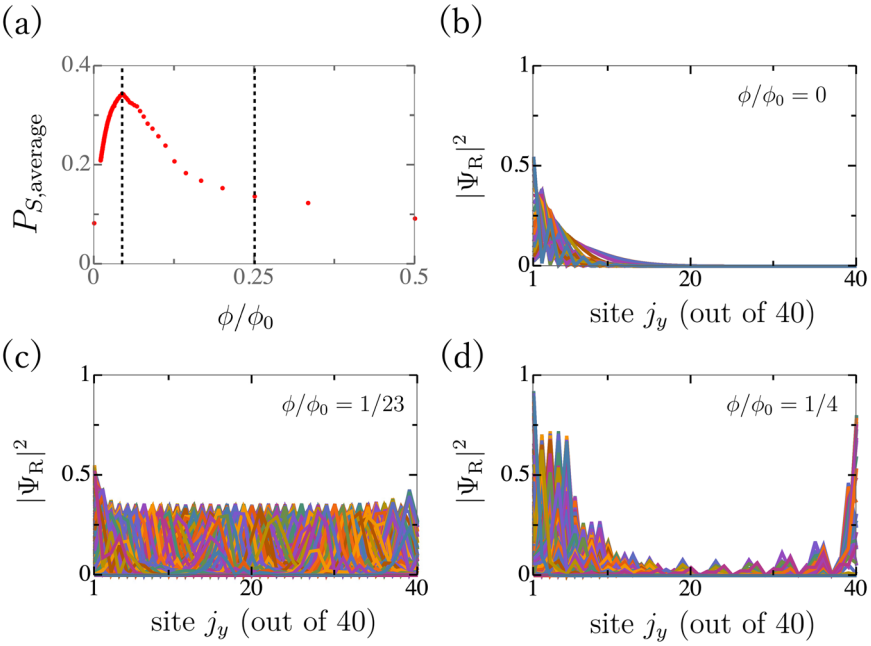

Fig. 4 | Magnetic suppression and recovery of skin localization. a Static polarization averaged over k_x at fluxes $\phi/\phi_0 = 1/\nu$ with $\nu = 2, \ldots, 100$ and $\phi = 0$. Dashed lines indicate $\phi/\phi_0 = 1/23, 1/4$. **b–d** Spatial profile of the right eigenstates of X for all momenta in the average. The fluxes are $\phi/\phi_0 = 0$ in (**a**), $\phi/\phi_0 = 1/23$ in (**b**), and $\phi/\phi_0 = 1/4$ in (**c**). We use dissipation strength $\gamma^l = 0.2$, $\gamma^s = 0$, hoppings $t_x = t_y = 1$, and lattice length $L_y = 40$.

Bloch states[49], which also affects chiral damping[45]. In agreement with this result, we observe that $P_{S,\text{average}}$, the spectral polarization averaged over 40 equidistant k_x-momenta, rapidly increases as the magnetic field is switched on, see Fig. 4a. When the flux per plaquette reaches intermediate values, however, the localization profile of eigenstates changes, see Fig. 4b–d. We find that an extensive skin localization is recovered at intermediate fluxes, rendering chiral damping observable again. In small flux regimes[49], applying a magnetic field can suppress the NHSE by pushing skin modes from the boundary back into the bulk. This suppression occurs because the magnetic field restores the standard bulk description that is otherwise invalidated by non-Bloch skin modes. Intuitively, this suppression must eventually cease, particularly upon reaching a full flux quantum, at which point the global skin effect is reinstated. While the precise dynamics of skin localization restoration at intermediate fluxes require further theoretical investigation, our numerical calculations confirm the validity of this behavior.

Conclusions

We find that the dynamics of particle densities in open quantum systems enables a direct visualization of coexisting spectral and band topologies. In particular, we show that the non-Hermitian skin effect, a paradigmatic example of spectral topology, can dominate the short-time dynamics, while band topology can protect topological edge states governing the long-time dynamics. The measurable consequence thereof is a combination of chiral damping at short times and edge-selective extremal damping at long times. We explain that the decoupling of chiral damping and edge-selective extremal damping in time is due to their separate origins (non-reciprocal hopping vs. edge-specific damping). Further, if we have open boundary conditions in both the directions, we expect a dynamical corner localization at late times. This is because the edges which had a nontrivial point-gap topology, under PBC along one direction, when opened up give rise to the corner skin-localization along the corresponding direction.

While we discuss these results with the example of a dissipative Hofstadter model, in which the individual analysis of spectral and band topologies is particularly illuminating, our findings provide insights into the interplay of spectral and band topologies in the dynamics of open topological quantum systems more generally. Our results are applicable to the vast class of topological systems with bond dissipators inducing a skin effect, and hence not model specific. Our findings unveil how the non-Hermitian skin effect and topological edge states affect the dynamics of such systems, an important step given that, arguably, most natural realizations of non-Hermitian phenomena are in dynamical systems with physical loss or gain in time. As such, our results directly connect to experiments in artificially engineered topological systems, e.g., in waveguides or electric circuits[50,51]. Ultracold atoms[52], where signatures of skin effect have been reported is also a promising platform for simulating open quantum systems such as ours. Beyond these general findings, our study also considerably deepens the understanding of how magnetic fields impact open quantum systems. This is important given the experimental relevance of magnetic fields as a tuning knob.

Data availability

All data supporting the findings of this study are included within the article and the supplementary information.

Code availability

Computer codes used for calculations and generation of figures are available upon request.

Received: 4 August 2025; Accepted: 23 February 2026;
Published online: 18 March 2026

References

1. Xie, B.-Y. et al. Photonics meets topology. *Opt. Express* **26**, 24531 (2018).
2. Ozawa, T. et al. Topological photonics. *Rev. Mod. Phys.* **91**, 015006 (2019).
3. Ma, G., Xiao, M. & Chan, C. T. Topological phases in acoustic and mechanical systems. *Nat. Rev. Phys.* **1**, 281 (2019).
4. Lo, P.-W. et al. Topology in nonlinear mechanical systems. *Phys. Rev. Lett.* **127**, 076802 (2021).
5. Shankar, S., Souslov, A., Bowick, M. J., Marchetti, M. C. & Vitelli, V. Topological active matter. *Nat. Rev. Phys.* **4**, 380 (2022).
6. Akin, E. *The General Topology of Dynamical Systems*, vol. 1 (American Mathematical Soc., 1993). https://doi.org/10.1090/gsm/001.
7. Bardyn, C.-E. et al. Topology by dissipation. *N. J. Phys.* **15**, 085001 (2013).
8. Gneiting, C., Koottandavida, A., Rozhkov, A. V. & Nori, F. Unraveling the topology of dissipative quantum systems. *Phys. Rev. Res.* **4**, 023036 (2022).

9. Martinez Alvarez, V., Barrios Vargas, J. & Foa Torres, L. Non-hermitian robust edge states in one dimension: Anomalous localization and eigenspace condensation at exceptional points. *Phys. Rev. B* **97**, 121401 (2018).
10. Yao, S. & Wang, Z. Edge states and topological invariants of non-hermitian systems. *Phys. Rev. Lett.* **121**, 086803 (2018).
11. Zhang, K., Yang, Z. & Fang, C. Correspondence between winding numbers and skin modes in non-Hermitian systems. *Phys. Rev. Lett.* **125**, 126402 (2020).
12. Bergholtz, E. J., Budich, J. C. & Kunst, F. K. Exceptional topology of non-hermitian systems. *Rev. Mod. Phys.* **93**, 015005 (2021).
13. Borgnia, D. S., Kruchkov, A. J. & Slager, R.-J. Non-hermitian boundary modes and topology. *Phys. Rev. Lett.* **124**, 056802 (2020).
14. Lin, R., Tai, T., Li, L. & Lee, C. H. Topological non-hermitian skin effect. *Front. Phys.***18** https://doi.org/10.1007/s11467-023-1309-z (2023).
15. McDonald, A., Hanai, R. & Clerk, A. A. Nonequilibrium stationary states of quantum non-hermitian lattice models. *Phys. Rev. B* **105**, 064302 (2022).
16. Lee, G., McDonald, A. & Clerk, A. Anomalously large relaxation times in dissipative lattice models beyond the non-hermitian skin effect. *Phys. Rev. B* **108**, 064311 (2023).
17. Song, F., Yao, S. & Wang, Z. Non-hermitian skin effect and chiral damping in open quantum systems. *Phys. Rev. Lett.* **123**, 170401 (2019).
18. Yang, F., Jiang, Q.-D. & Bergholtz, E. J. Liouvillian skin effect in an exactly solvable model. *Phys. Rev. Res.* **4**, 023160 (2022).
19. Yao, S., Song, F. & Wang, Z. Non-Hermitian Chern bands. *Phys. Rev. Lett.* **121**, 136802 (2018).
20. Hegde, S. S., Ehmcke, T. & Meng, T. Edge-selective extremal damping from topological heritage of dissipative Chern insulators. *Phys. Rev. Lett.* **131**, 256601 (2023).
21. Cherifi, W., Carlström, J., Bourennane, M. & Bergholtz, E. J. Non-Hermitian Boundary State Distillation with Lossy Waveguides. arXiv: 2304.03016. https://arxiv.org/abs/2304.03016 (2023).
22. Yang, F., Molignini, P. & Bergholtz, E. J. Dissipative boundary state preparation. *Phys. Rev. Res.* **5**, 043229 (2023).
23. Zhu, W., Teo, W. X., Li, L. & Gong, J. Delocalization of topological edge states. *Phys. Rev. B* **103**, 195414 (2021).
24. Cheng, J., Zhang, X., Lu, M.-H. & Chen, Y.-F. Competition between band topology and non-hermiticity. *Phys. Rev. B* **105**, 094103 (2022).
25. Zhu, W. & Gong, J. Hybrid skin-topological modes without asymmetric couplings. *Phys. Rev. B* **106**, 035425 (2022).
26. Wang, W., Wang, X. & Ma, G. Non-hermitian morphing of topological modes. *Nature* **608**, 50–55 (2022).
27. Li, B., Wang, H.-R., Song, F. & Wang, Z. Non-Bloch dynamics and topology in a classical nonequilibrium process. *Phys. Rev. B* **109**, L201121 (2024).
28. Zelenayova, M. & Bergholtz, E. J. Non-hermitian extended midgap states and bound states in the continuum. *Appl. Phys. Lett.***124** https://doi.org/10.1063/5.0184935 (2024).
29. Hofstadter, D. R. Energy levels and wave functions of Bloch electrons in rational and irrational magnetic fields. *Phys. Rev. B* **14**, 2239–2249 (1976).
30. Lindblad, G. On the generators of quantum dynamical semigroups. *Commun. Math. Phys.* **48**, 119 (1976).
31. Breuer, H.-P. & Petruccione, F. *The Theory of Open Quantum Systems* (Oxford University Press, 2007). https://doi.org/10.1093/acprof:oso/9780199213900.001.0001.
32. Hatano, N. & Nelson, D. R. Localization transitions in non-hermitian quantum mechanics. *Phys. Rev. Lett.* **77**, 570–573 (1996).
33. Yokomizo, K. & Murakami, S. Non-Bloch band theory of non-Hermitian systems. *Phys. Rev. Lett.* **123**, 066404 (2019).
34. Nakamura, D., Inaka, K., Okuma, N. & Sato, M. Universal platform of point-gap topological phases from topological materials. *Phys. Rev. Lett.* **131**, 256602 (2023).
35. Haga, T., Nakagawa, M., Hamazaki, R. & Ueda, M. Liouvillian skin effect: Slowing down of relaxation processes without gap closing. *Phys. Rev. Lett.* **127**, 070402 (2021).
36. Minganti, F., Biella, A., Bartolo, N. & Ciuti, C. Spectral theory of Liouvillians for dissipative phase transitions. *Phys. Rev. A* **98**, 042118 (2018).
37. Ughrelidze, M., Flynn, V. P., Cobanera, E. & Viola, L. Interplay of finite- and infinite-size stability in quadratic bosonic Lindbladians. *Phys. Rev. A* **110**, 032207 (2024).
38. Purkayastha, A., Sanyal, S., Dhar, A. & Kulkarni, M. Anomalous transport in the aubry-andré-harper model in isolated and open systems. *Phys. Rev. B* **97**, 174206 (2018).
39. Longhi, S. Topological phase transition in non-hermitian quasicrystals. *Phys. Rev. Lett.* **122**, 237601 (2019).
40. Zhang, D.-W. et al. Skin superfluid, topological Mott insulators, and asymmetric dynamics in an interacting non-Hermitian aubry-andré-harper model. *Phys. Rev. B* **101**, 235150 (2020).
41. Zeng, Q.-B., Yang, Y.-B. & Xu, Y. Topological phases in non-hermitian aubry-andré-harper models. *Phys. Rev. B* **101**, 020201 (2020).
42. Longhi, S. Phase transitions in a non-Hermitian aubry-andré-harper model. *Phys. Rev. B* **103**, 054203 (2021).
43. Liu, Y., Zhou, Q. & Chen, S. Localization transition, spectrum structure, and winding numbers for one-dimensional non-hermitian quasicrystals. *Phys. Rev. B* **104**, 024201 (2021).
44. Tang, L.-Z., Zhang, G.-Q., Zhang, L.-F. & Zhang, D.-W. Localization and topological transitions in non-hermitian quasiperiodic lattices. *Phys. Rev. A* **103**, 033325 (2021).
45. He, P., Liu, Y.-G., Wang, J.-T. & Zhu, S.-L. Damping transition in an open generalized aubry-andré-harper model. *Phys. Rev. A* **105**, 023311 (2022).
46. Mallick, A., Andreanov, A. & Flach, S. Intermediate superexponential localization with aubry-andré chains. *Phys. Rev. B* **108**, 064204 (2023).
47. Zhou, L. Entanglement phase transitions in non-hermitian quasicrystals. *Phys. Rev. B* **109**, 024204 (2024).
48. Padhi, S. R., Padhan, A., Banerjee, S. & Mishra, T. Quasiperiodic and periodic extended Hatano-Nelson model: Anomalous complex-real transition and non-hermitian skin effect. *Phys. Rev. B* **110**, 174203 (2024).
49. Lu, M., Zhang, X.-X. & Franz, M. Magnetic suppression of non-hermitian skin effects. *Phys. Rev. Lett.* **127**, 256402 (2021).
50. Imhof, S. et al. Topolectrical-circuit realization of topological corner modes. *Nat. Phys.* **14**, 925–929 (2018).
51. Rotter, I. & Bird, J. A review of progress in the physics of open quantum systems: theory and experiment. *Rep. Prog. Phys.* **78**, 114001 (2015).
52. Liang, Q. et al. Dynamic signatures of non-hermitian skin effect and topology in ultracold atoms. *Phys. Rev. Lett.* **129**, 070401 (2022).

Acknowledgements

RS is supported by the Prime Minister's Research Fellowship (PMRF). AN acknowledges support from the DST MATRICS grant (MTR/2023/000021). SH and TM acknowledge funding by the Deutsche Forschungsgemeinschaft (DFG) via the Emmy Noether Program (Quantum Design grant, ME4844/1, project-id 327807255), project A04 of the Collaborative Research Center SFB 1143 (project-id 247310070), and the Cluster of Excellence on Complexity and Topology in Quantum Matter ct.qmat (EXC 2147, project-id 390858490). SH further acknowledges funding support from ANRF grant no: ANRF/ECRG/2024/002083/PMS.

Author contributions

RS, SH, AN and TM conceived the study. RS and SH performed the calculations. RS, SH, AN and TM analysed and interpreted the simulation data, and wrote the manuscript.

Funding

Open Access funding enabled and organized by Projekt DEAL.

Competing interests
The authors declare no competing interests.

Additional information
Supplementary information The online version contains supplementary material available at https://doi.org/10.1038/s42005-026-02573-z.

Correspondence and requests for materials should be addressed to Tobias Meng.

Peer review information *Communications Physics* thanks the anonymous reviewers for their contribution to the peer review of this work. A peer review file is available.